Synchronizing Terahertz Wave Generation with Attosecond Bursts

Dongwen Zhang, Zhihui Lü, Chao Meng, Xiyu Du, Zhaoyan Zhou, Zengxiu Zhao,* and Jianmin Yuan†

Department of Physics, National University of Defense Technology, Changsha 410073, People's Republic of China

(Received 18 June 2012; published 10 December 2012)

We perform a joint measurement of terahertz waves and high-harmonics generated from argon atoms driven by a fundamental laser pulse and its second harmonic. By correlating their dependence on the phase delay between the two pulses, we determine the generation of THz waves in tens of attoseconds precision. Compared with simulations and models, we find that the laser-assisted soft collision of the electron wave packet with the atomic core plays a key role. It is demonstrated that the rescattering process, being indispensable in high-harmonic generation processes, dominates THz wave generation as well in a more elaborate way. The new finding might be helpful for the full characterization of the rescattering dynamics.

DOI: 10.1103/PhysRevLett.109.243002 PACS numbers: 33.20.Xx, 32.80.Qk

Intense terahertz (THz) radiation from ionizing gases in two-color laser fields has attracted great interest recently, not only for the applications, such as remote sensing [1], but also for understanding the mechanism of terahertz generation [2–14]. When the fundamental and frequency-doubled femtosecond laser pulses are focused in gases, the intensity of the THz radiation is modulated by the relative phase between the two pulses. Experiments confirm that THz output increases dramatically with the onset of plasma formation, indicating that ionization plays a key role in THz wave generation (TWG) [3,4]. Four-wave mixing (FWM) in plasma was suggested to elucidate the extreme nonlinear phenomenon but without the knowledge of the origin of $\chi^{(3)}$ responsible for such high efficiency.

A transient photoelectron current (PC) model is recently proposed by considering the subsequent electron dynamics following ionization [7,8]. In this model, electrons are released from atoms through tunnel ionization and then driven by a nonsinusoidal two-color laser field that breaks the dynamic symmetry of the electronic wave packet (EWP). A directional current is thus formed that is responsible for TWG. However, there is a discrepancy between the above models on the optimal phase delay when terahertz yield maximizes, respectively, at 0 and 0.5π in FWM and PC models. It is evident that the key problem of describing TWG in two-color fields is to find the buildup process and the subsequent relaxation of the transient current [6,8,13,14]. The sensitivity to the phase delay indicates that the subcycle electron dynamics needs to be measured to understand TWG, and a determination of the relative phase in attosecond precision is urgently expected.

It is known that a commensurate two-color field can be used to steer trajectories of continuum electrons and to control their rescattering or recollision with the parent ion to manipulate high-harmonic generation (HHG) [15–19]. In HHG processes, each harmonic can be uniquely related to two quantum orbits within each optical cycle based on the rescattering theory [20]. Two-photon ionization experiments have confirmed that the emission time of harmonics differs in attoseconds, and the resulting attosecond bursts are positively chirped for short trajectories [21–23]. The weak second-harmonic field tunes the phase difference of radiation bursts generated in the positive and negative half-cycle of the fundamental, causing the appearance of even harmonics with intensity modulated by the phase delay between the two pulses [24,25]. The two-color scheme thus provides an all-optical *in situ* method for measuring the birth of extreme ultraviolet pulses [17], which is an ideal clock for timing TWG in attoseconds. Furthermore, since both yields of THz waves and harmonics modulate when the time delay between the two pulses varies by attoseconds, a question arises: how they are related in view of THz pulses lasting for picoseconds?

We therefore perform a joint measurement by monitoring THz and high-harmonic yields in a two-color laser field simultaneously. By correlating their phase-delay dependence, the absolute phase delay can be retrieved, and it is found that THz yields take a maximum at the phase delay of 0.8π deviated from the predictions of the FWM (0) and the PC (0.5π) models [7,8]. By analyzing electron dynamics classically and quantum mechanically, we find that the Coulomb potential of the residual ion can not be neglected. It is shown that the laser-assisted soft collision of the EWP with the atomic core induces a momentum transfer to the electron affecting the phase dependence of THz yields.

In the experiment, we used a 1 kHz Ti:sapphire chirped pulse amplification system that delivered 1.6 mJ at 790 nm in a 25 fs pulse. The beam is reduced to a diameter of 10 mm and split into pump and probe beams. The pump is directed on a 200 μm thick β-barium borate crystal (type I) to generate the second-harmonic beam with 20% conversion efficiency. A two-color Mach-Zehnder interferometer is employed to control the relative phase between the two pulses, with a pair of fused-silica wedges in the fundamental path. Neutral density filters are used in both arms to control their intensities separately. High-harmonics and THz waves are generated in a 1.5 mm long gas cell in 12 mbar by the two-color pulse using an off-axis parabolic

Au-coated mirror with a focal length of 200 mm. The gas cell is placed 2.5 mm behind the focus to optimize the HHG yields. The THz waves are reflected with a hole-drilled off-axis parabolic mirror and then combined with the delayed probe beam into a 1 mm thick (110)-cut ZnTe crystal for electro-optic sampling (EOS) the waveform below 3 THz. The harmonics passing the hole is simultaneously recorded by a homemade flat-field spectrometer for each phase delay.

In Fig. 1, we show the measured THz wave forms and the yields of high harmonics modulated with the phase delay between the fundamental pulse (E_1) and the second-harmonic (E_2) pulse. The total field is characterized by $E(t) = E_1 \cos\omega t + E_2 \cos(2\omega t + \phi)$, where the phase delay is related to the time delay by $\phi = 2\omega t_d$. The solid line depicts the optimal phase delay, maximizing the yields of even harmonics from 16th to 26th order. In order to determine the absolute phase delay, we apply the procedure given in Ref. [17] by mapping the optimal phase to the emission time of harmonics obtained from the rescattering model [20]. The intensity of the $2N$th harmonic is modulated approximately as $\sin^2\Delta$, where Δ is the additional action introduced by the vector potential of the second-harmonic pulse and is given by [16,17] $\Delta \approx \lambda E_1^2/2\omega^2 \int_{t_i}^{t_r} (\sin\omega t - \sin\omega t_i)\sin(2\omega t + \phi)dt$, with the ionization instant t_i and the recombination instant t_r as functions of harmonic energy and λ as the ratio of E_2 to E_1. The corresponding phase delay that maximizes $2N$th harmonic yields is plotted in solid lines in Fig. 2. Also shown in Fig. 2 are the extracted experimental data, denoted in circles. The lower harmonic reaches its maximum at a later delay, in accordance with the HHG from short trajectories [21]. Note that the left part of the theoretical result (solid line) corresponds to the case of HHG from the long trajectories that has been removed by phase matching in experiments. The overall agreement between theory and experiment for all the harmonics presented allows us to determine the absolute phase delay maximizing yields of harmonics; e.g., the 22nd harmonic takes its maximum at 0.93π. Less than a 0.04π phase-delay control is achieved in the experiment, corresponding to 60 as. Now, using the harmonic modulation as ticks, we can assign the absolute phase delay to the modulation of THz yields (pulse energy) shown in Fig. 2. Because the THz and harmonic yields are measured jointly for each given phase delay, we can in fact lock the modulation of THz yield to any of the even harmonics. The THz yield peaks at the phase delay of 0.8π. Using the quantum mechanical approach [9,26], we obtain the same result, which deviates from the predictions of the FWM (0) and the PC (0.5π) models.

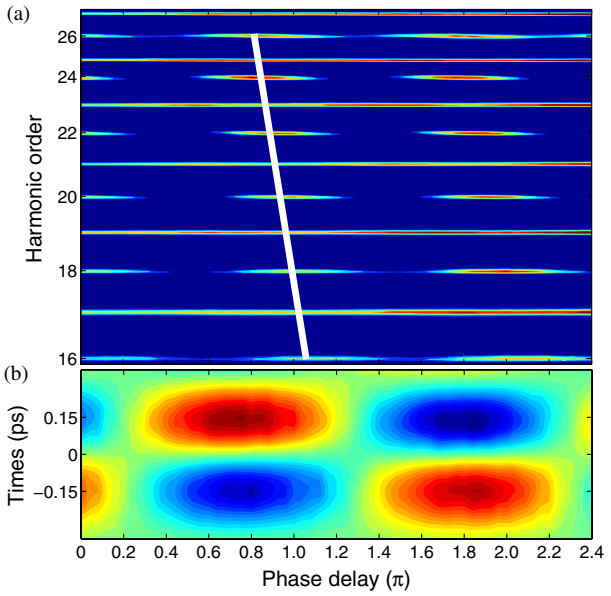

FIG. 1 (color online). Contours of the terahertz wave forms (b) and the intensities of harmonics (a) varying with the phase delay between the two-color laser fields. The intensity ratio of the second harmonic to the fundamental field is about 0.5%.

According to the photoelectron current model, the microscopic current $j(t_i)$ generated from the ionization event at time t_i can be obtained by weighting the final outgoing electron velocity with the corresponding instantaneous ionization rate [7]. The initial velocity of the electron born at time t_i is assumed zero, and the final electron velocity can be found from the classical electron motion in laser fields. The total current responsible for THz emission is thus the coherent summation over all the ionization events. Because the microscopic currents generated from two ionization events separated by π/ω have the symmetry of $j(t_i) = -j(t_i + \pi/\omega)$, their destructive interference causes vanishing total currents for TWG in a single-color laser field. When a second-harmonic pulse is introduced, the symmetry between t_i and $t_i + \pi/\omega$ is broken, and directional current is formed, causing TWG.

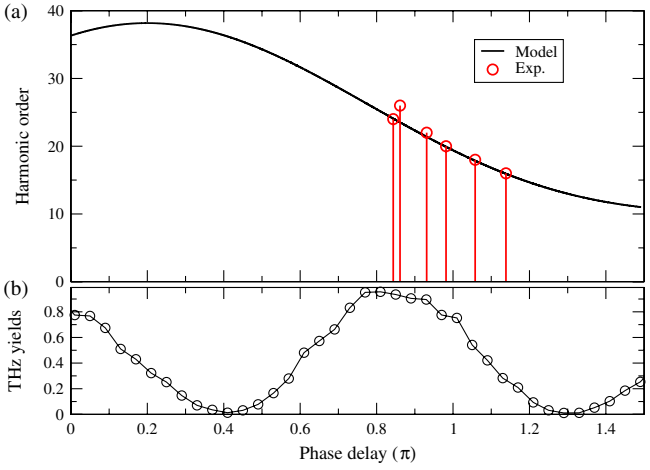

FIG. 2 (color online). (a) The phase delay extracted from the experiment (circles) and the theoretical model (solid line), which maximizes the intensity of even harmonics. (b) Modulation of THz yields with phase delay. The fundamental laser intensity is estimated to be 2.3×10^{14} W/cm^2.

Depending on the instant when it is set free, the electron can either directly escape from the atom or recollide with the atomic core. We can therefore define the escaping currents (EC) and rescattering currents (RC), $j_{esc}(t_i)$ and $j_{res}(t_i)$, accordingly. Because of the high energy gained from the laser field by electrons approaching the core, HHG is mainly contributed by the high frequency components of the RC. On the contrary, the THz wave has a photon energy in meVs: it can be emitted at much larger distances from the nucleus involving free-free transitions [26]. Therefore, the contributions of low-energy and less-accelerated electrons can not be ruled out and the EC needs to be considered as well. Note that EC (RC) is related to tunnel ionization occurring in the quarter cycles before (after) the electric field maxima. Because $j_{res}(t_i) = -j_{esc}(-t_i)$, the magnitude of the total current from a two-color laser pulse takes its maximum at the relative phase of $\pi/2$ [8].

In the above discussion regarding free-electron motion, only the electron-light interaction is considered, while the influence of the Coulomb potential from the residue atomic core is neglected completely. This so-called strong field approximation [20] has been widely used in modeling processes such as HHG where high-kinetic-energy electrons are involved. However, for near-threshold phenomena, it can distort the free-electron wave function significantly and modify the density of states [27], causing Coulomb focusing effects in double ionization [28]. The Coulomb-laser coupling has been shown affecting laser-assisted photoionization [29], ellipticity dependence of low harmonics [30], angular distribution [31], and low-energy peaks of above-threshold ionization (ATI) photoelectrons [32], as well. Since TWG involves slow electron motion that can be strongly distorted by the Coulomb potential, the response of the whole EWP under Coulomb-laser coupling needs to be investigated. In the following, we show that the Coulomb potential has impacts on the formation of the EC and the RC.

We consider two kinds of electron trajectories that start from two respective ionization instants $t_1 = 0.075$ fs and $t_2 = -0.15$ fs in the two-color laser pulse, with form given above at zero phase delay. Both the fundamental and the second-harmonic pulses have a Gaussian envelope with a duration of 25 fs and intensities of 1 and 0.05 in units of 10^{14} W/cm^2, respectively. The corresponding classical trajectories of the electron driven solely by the laser field are shown in the dotted lines in Figs. 3(a) and 3(d), respectively. Quantum mechanically, we propagate the continuum EWP following tunneling ionization. The initial EWPs at the instants of tunneling ionization are assumed to have the same shape of the ground state wave function but are shifted to the classical turning points at $x_0 = -I_p/E$, where I_p is the ionization potential and E is the corresponding instantaneous electric field. The one-dimensional time-dependent Schrödinger equation (TDSE) is solved for simplicity. The evolution of the EWPs in the absence of the Coulomb potential is shown in Figs. 3(b) and 3(e), respectively.

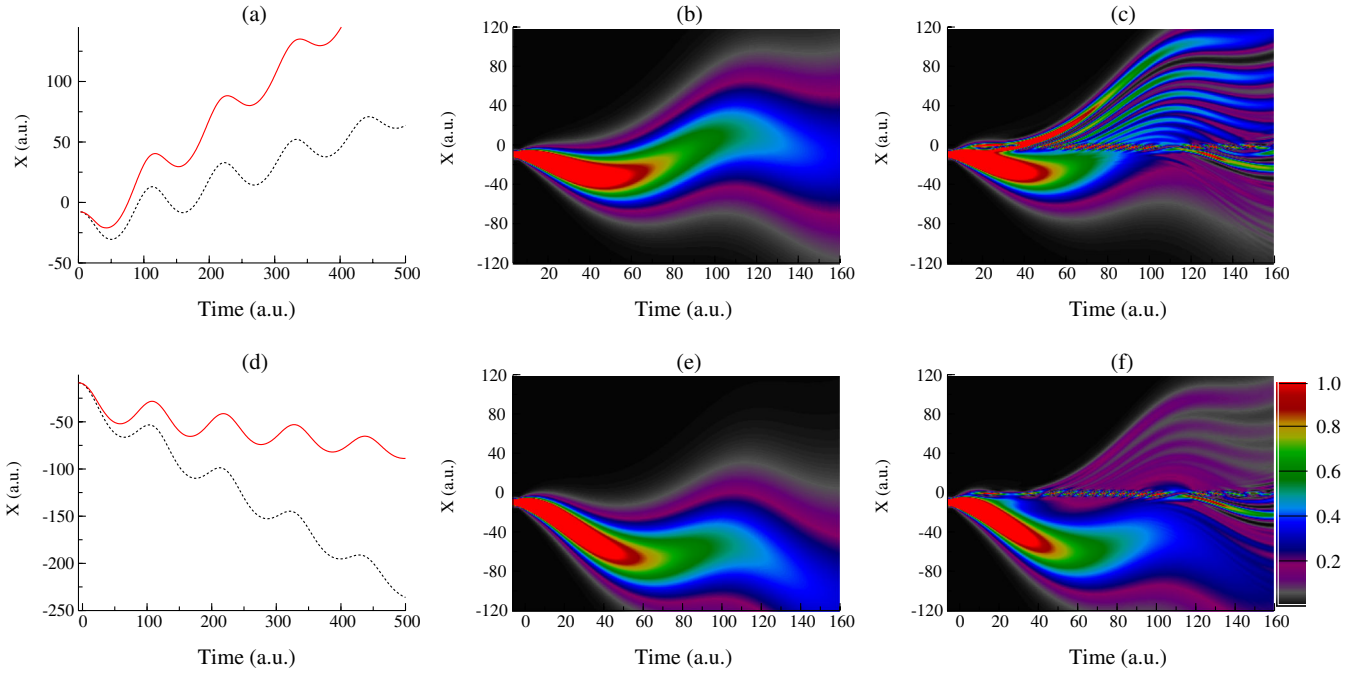

FIG. 3 (color online). Time propagation of EWPs after tunneling ionization at two instants t_1 (top) and t_2 (bottom) corresponding to the scenarios of rescattering and escaping, respectively. The dotted lines in (a) and (d) represent the classical trajectories of electrons with zero initial velocity, and the solid lines represent the quantum mechanical averaged electron displacements. The contour plots (b), (c) and (e),(f) show the time evolution of the probability density, with (without) the Coulomb potential being considered in (c) and (f) [(b) and (e)]. A linear color scale is used, with 1.0 corresponding to the density of 0.02 a.u.

As one of the quantum features, the EWPs are broadened during evolution because of the quantum dispersion. However, the center motion of the EWP coincides exactly with the classical motion of the electron in a laser field with zero initial momentum. The wave packet shown in Fig. 3(b) moves toward the negative X axis initially and then turns back to the positive axis, passing the origin where the atomic core is positioned. It is obviously the scenario of rescattering. The central part of the EWP makes hard collision with the atomic core that causes HHG and high-energy ATI when followed by either recombination or backscattering [33]. However, the THz yields are determined by the ejecting photoelectron current; therefore, we must consider the propagation of the wave packet after being scattered by the atomic potential. As seen in Fig. 3(c), the EWP is fragmented after recolliding with the atomic core. Especially, the upper wing of the EWP is strongly enhanced in density, comparable to that of the center. The magnitude of the averaged velocity is increased because of more fractions of electrons moving toward the positive direction. The averaged displacement plotted in the solid line in Fig. 3(a) demonstrates that the photoelectron current is indeed enhanced. Different from recombination and backscattering processes, here the evolution of the whole EWP is considered with most of the packet scattered away from the atom. In other words, it is the laser-driven soft collision of the EWPs with an atomic core that causes the enhancing of the RC. It might be the same mechanism that causes low-energy peaks in photoelectron spectra [34]. On the contrary, in Fig. 3(e), the center of the EWP quivers away from the origin, without the chance of reencountering the atomic core to make hard collisions. Due to the broadening of the EWP, fractions of electrons in the wing of the EWP pass through the origin, but the averaged velocity of the electron makes no change when the atomic potential is ignored. If the Coulomb potential is included in the time propagation, we can see in Fig. 3(f) that the wing of the EWP is altered by the atomic core. It is fragmented as well with more fractions of electrons moving toward the positive axis by the attractive Coulomb potential. Because the total drift velocity is negative in the absence of the Coulomb potential, it is suppressed, as plotted in the solid line compared with the dotted line in Fig. 3(d). The soft collision with the atomic core thus reduces the EC.

The laser-assisted soft collision mainly occurs within the first quarter cycle following ionization because the electron drifts away from the nucleus at a later time when the effect of the Coulomb potential is no longer significant. At the instant when the electron makes the turn, the momentum transfer is most probable since the electron has more time interacting with the Coulomb potential due to the zero velocity. It can be investigated theoretically from the classical electron motion under the coupling of the atomic potential and the laser field [29,35]. In the case of rescattering, our estimation gives an approximate momentum transfer of $\Delta\vec{p} \approx 2\vec{E}/\kappa^3$, where $\kappa = \sqrt{2I_p}$ and $\vec{E}$ is the field at the instant of ionization. Because of the momentum transfer by the Coulomb potential, the symmetry between the EC and the RC is broken, with the former suppressed and the latter enhanced. Therefore, the rescattering process dominates TWG as well but because of the laser-driven soft collision of the EWP with the atomic core.

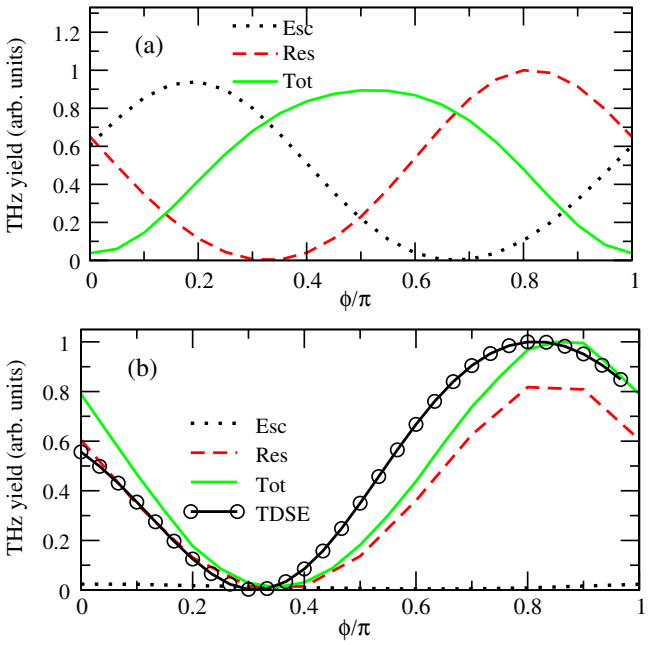

FIG. 4 (color online). (a) THz yields by the escaping, the rescattering, and the total currents calculated from the photocurrent model and (b) THz yields obtained from classical EWP simulation by considering Coulomb potential and from solving TDSE with the same laser parameters given in Fig. 3.

In order to further check the analysis above, we perform classical and quantum calculations for the TWG in a two-color laser pulse. In the classical EWP simulation, the electron current is found by sampling and tracing the trajectories with Gaussian distributed initial transversal momenta according to the tunneling ionization theory [36]. In the quantum simulation, the time-varying dipole acceleration is obtained from solving the 1D TDSE with the soft-core Coulomb potential [37]. The total power emitted within 0–30 THz from the Fourier transformed dipole acceleration is used to indicate the phase-delay dependence. As shown in Fig. 4(a), the THz yield takes its maximum at a phase delay of 0.5π from the photocurrent model, which ignores the Coulomb potential. When the Coulomb potential is taken into account in the classical EWP simulation shown in Fig. 4(b), the THz yield from the EC is suppressed while that from the RC is enhanced. The total THz yield takes its maximum at the phase delay of 0.8π, which agrees with the TDSE calculation, confirming the previous discussion. It is known that the THz spectrum is determined by the formation of the current [37], the decay of the current by collision [14], and the possible excitation of plasma oscillation [6]. In this Letter, we have

omitted the latter two processes, which are found to be less dependent on the phase delay [10] based on the similarity of the THz waveform measured by EOS techniques [38].

In conclusion, the joint measurement of THz and harmonic yields allows us to determine the generation of THz waves in attosecond precision. We show that the hard collision with the atomic core leads to HHG upon recombination, and the soft collision with the atomic core gives rise to THz photocurrents. We expect that the sensitivity of THz yields to the Coulomb potential could be used to map atomic fields from within and to help the full characterization of the rescattering wave packet, beyond the recombination in HHG and the backscattering in ATI.

This work is supported by the National Basic Research Program of China (973 Program) under Grant No. 2013CB922203, the NSF of China (Grant No. 11104352), the Major Research Plan of the NSF of China (Grant No. 91121017), and the National High-Tech ICF Committee of China.

*zhao.zengxiu@gmail.com
†jmyuan@nudt.edu.cn

[1] J. Liu, J. Dai, S. L. Chin, and X.-C. Zhang, Nat. Photonics **4**, 627 (2010).
[2] D. J. Cook and R. M. Hochstrasser, Opt. Lett. **25**, 1210 (2000).
[3] M. Kress, T. Löffler, S. Eden, M. Thomson, and H. G. Roskos, Opt. Lett. **29**, 1120 (2004).
[4] M. Kress *et al.*, Nat. Phys. **2**, 327 (2006).
[5] X. Xie, J. Dai, and X.-C. Zhang, Phys. Rev. Lett. **96**, 075005 (2006).
[6] V. B. Gildenburg and N. V. Vvedenskii, Phys. Rev. Lett. **98**, 245002 (2007).
[7] K. Y. Kim, J. H. Glownia, A. J. Taylor, and G. Rodriguez, Opt. Express **15**, 4577 (2007).
[8] K. Y. Kim, A. J. Taylor, J. H. Glownia, and G. Rodriguez, Nat. Photonics **2**, 605 (2008).
[9] A. A. Silaev and N. V. Vvedenskii, Phys. Rev. Lett. **102**, 115005 (2009).
[10] H. Wen and A. M. Lindenberg, Phys. Rev. Lett. **103**, 023902 (2009).
[11] Y. Chen, C. Marceau, S. Genier, F. Theberge, M. Châteauneuf, J. Dubois, and S. L. Chin, Opt. Commun. **282**, 4283 (2009).
[12] J. Dai, N. Karpowicz, and X.-C. Zhang, Phys. Rev. Lett. **103**, 023001 (2009).
[13] I. Babushkin, W. Kuehn, C. Köhler, S. Skupin, L. Bergé, K. Reimann, M. Woerner, J. Herrmann, and T. Elsaesser, Phys. Rev. Lett. **105**, 053903 (2010).
[14] V. A. Kostin and N. V. Vvedenskii, Opt. Lett. **35**, 247 (2010).
[15] D. A. Telnov, J. Wang, and S.-I. Chu, Phys. Rev. A **52**, 3988 (1995).
[16] C. F. de Morisson Faria, M. Dörr, W. Becker, and W. Sandner, Phys. Rev. A **60**, 1377 (1999).
[17] N. Dudovich, O. Smirnova, J. Levesque, Y. Mairesse, M. Y. Ivanov, D. M. Villeneuve, and P. B. Corkum, Nat. Phys. **2**, 781 (2006).
[18] H. Mashiko, S. Gilbertson, C. Li, S. D. Khan, M. M. Shakya, E. Moon, and Z. Chang, Phys. Rev. Lett. **100**, 103906 (2008).
[19] X. Feng, S. Gilbertson, H. Mashiko, H. Wang, S. D. Khan, M. Chini, Y. Wu, K. Zhao, and Z. Chang, Phys. Rev. Lett. **103**, 183901 (2009).
[20] M. Lewenstein, P. Balcou, M. Y. Ivanov, A. L'Huillier, and P. B. Corkum, Phys. Rev. A **49**, 2117 (1994).
[21] P. M. Paul, E. S. Toma, P. Breger, G. Mullot, F. Auge, P. Balcou, H. G. Muller, and P. Agostini, Science **292**, 1689 (2001).
[22] Y. Mairesse *et al.*, Science **302**, 1540 (2003).
[23] S. A. Aseyev, Y. Ni, L. J. Frasinski, H. G. Muller, and M. J. J. Vrakking, Phys. Rev. Lett. **91**, 223902 (2003).
[24] J. Mauritsson, P. Johnsson, E. Gustafsson, A. L'Huillier, K. J. Schafer, and M. B. Gaarde, Phys. Rev. Lett. **97**, 013001 (2006).
[25] Y. Oishi, M. Kaku, A. Suda, F. Kannari, and K. Midorikawa, Opt. Express **14**, 7230 (2006).
[26] Z. Zhou, D. Zhang, Z. Zhao, and J. Yuan, Phys. Rev. A **79**, 063413 (2009).
[27] M. D. Perry, O. L. Landen, A. Szöke, and E. M. Campbell, Phys. Rev. A **37**, 747 (1988).
[28] T. Brabec, M. Y. Ivanov, and P. B. Corkum, Phys. Rev. A **54**, R2551 (1996).
[29] O. Smirnova, A. S. Mouritzen, S. Patchkovskii, and M. Y. Ivanov, J. Phys. B **40**, F197 (2007).
[30] M. Y. Ivanov, T. Brabec, and N. Burnett, Phys. Rev. A **54**, 742 (1996).
[31] J. Z. Kamiński, A. Jaroń, and F. Ehlotzky, Phys. Rev. A **53**, 1756 (1996).
[32] W. Quan *et al.*, Phys. Rev. Lett. **103**, 093001 (2009).
[33] G. G. Paulus, W. Becker, W. Nicklich, and H. Walther, J. Phys. B **27**, L703 (1994).
[34] A. Kästner, U. Saalmann, and J. M. Rost, Phys. Rev. Lett. **108**, 033201 (2012).
[35] O. Smirnova, M. Spanner, and M. Ivanov, Phys. Rev. A **77**, 033407 (2008).
[36] M. V. Ammosov, N. B. Delone, and V. P. Krainov, Zh. Eksp. Teor. Fiz. **91**, 2008 (1986) [Sov. Phys. JETP **64**, 1191 (1986)].
[37] A. A. Silaev, M. Y. Ryabikin, and N. V. Vvedenskii, Phys. Rev. A **82**, 033416 (2010). In the tunneling ionization regime, using various 1D model potentials gives similar phase-delay dependences, in contrast to their study on the carrier-envelope phase dependence of THz emission. It might be due to the less nonadiabatic excitation by the longer (25 fs) two-color laser pulses used in our work.
[38] The plasma frequency and the collision frequency are estimated to be 2 and 6 THz, respectively; therefore, the plasma oscillation is severely damped by the collision process. In fact, no distinct feature of plasma resonance is observed by EOS ($\nu_{\max} \approx 3$ THz) or by the air biased coherent detection scheme ($\nu_{\max} \approx 30$ THz). The THz spectrum is therefore mainly affected by the collisional process, but measurements at different pressures (below 40 mbar) barely show any variation of the phase correlation between HHG and THz, indicating that collisions do not affect the phase-delay dependence.